New approaches to the synthesis of anisotropic, core–shell and hollow metal nanostructures

Murali Sastry,* Anita Swami, Saikat Mandal and PR. Selvakannan

Received 22nd February 2005, Accepted 6th April 2005
First published as an Advance Article on the web 26th April 2005
DOI: 10.1039/b502704g

The synthesis of nanomaterials with control over size, shape and chemical composition continues to be a major challenge in nanoscience. The requirements of nanomaterial synthesis are becoming more sophisticated and, in addition to anisotropic structures, there is much excitement surrounding the development of recipes for the synthesis of core–shell and hollow nanostructures. Much of the motivation for research in this direction stems from the unusual optoelectronic and chemical properties exhibited by such nanostructures. In this article, we review the work from this laboratory on the synthesis of flat gold nanostructures at the air–water interface, either by confining the reductant or the precursor metal ions to the air–water interface. We also describe the synthesis of phase-pure core–shell nanoparticles by immobilizing UV- and pH-dependent reducing agents on the surface of the core nanoparticles as well as the synthesis of organically soluble hollow-shell nanostructures *via* transmetallation reactions.

Nanoscience Group, Materials Chemistry Division, National Chemical Laboratory, Pune, 411 008, India. E-mail: sastry@ems.ncl.res.in; Fax: +91 20 25893952/25893044; Tel: +91 20 25893044

Dr Murali Sastry

A PhD in physics from the Indian Institute of Technology Madras (now Chennai), Dr Murali Sastry heads the DST-NCL Unit of Nanoscience and Technology, a national centre of excellence in nanobiotechnology. Author of nearly 300 international publications and 7 chapters in books on nanoscience, he serves on the International Editorial Advisory Boards of Langmuir, Journal of Colloid and Interface Science, Journal of Biomedical Nanotechnology and Bulletin of Materials Science (Indian Academy of Sciences). His current research interests include synthesis and study of anisotropic and core–shell nanostructures, interfacing biology with nanomaterials with emphasis on biomedical applications, biomineralization and biological synthesis of inorganic materials.

Ms Anita Swami

Anita S. Swami completed her graduation in chemistry from the University of Pune. She has completed her PhD work under the guidance of Dr Murali Sastry. Her work is mainly focused on the synthesis and assembly of nanoparticles at the air–water interface and formation of superlattices of nanoparticle assemblies.

Mr PR. Selvakannan

PR. Selvakannan obtained his Bachelors and Masters degrees in chemistry from the American College, Madurai. Currently, he is a graduate student with Dr Murali Sastry, working in the area of chemical methods for the synthesis of metal nanoparticles of variable shape and in polymer composites.

Mr Saikat Mandal

Saikat Mandal was born in Chinsurah, India in 1976. He received the degree of Master of Science in 1999 at the Department of Chemistry, University of Calcutta. Currently, he has completed his PhD thesis under the supervision of Dr Murali Sastry. His work is concerned with the synthesis of metal and semiconductor nanoparticles in thin film form, core–shell nanostructures and assembly of metal nanoparticles using Keggin ions as an inorganic scaffold.

1. Introduction

Metal nanoparticles are being investigated in considerable detail due to their exciting potential for application in catalysis,[1] biological[2] and chemical sensing,[3] optoelectronics[4] and magnetic memory.[5] Hence, the development of reliable experimental procedures for the synthesis of nanomaterials over a range of chemical compositions and sizes constitutes an important area of research in nanotechnology. In addition to the size of nanoparticles, it is now recognized that nanoparticle shape plays a crucial role in determining their optical/electronic properties[6,7] as well as their catalytic activity.[8] Consequently, there is much current interest in developing experimental protocols for the synthesis of metal and semiconductor nanoparticles of different shapes. Nanorods/wires of silver[9] and gold,[10] nanoprisms (nanotriangles) and nanoplates of silver[6] and gold,[11] and tetrapods of gold[12] are some of the interesting metallic nanocrystalline shapes that can now be routinely synthesized in the laboratory. From a purely fundamental angle, the ability to control the shape of nanocrystals is particularly exciting and has led to the first observation of two distinct quadrupole plasmon resonance modes in silver nanoprisms.[6a] Distortion of the spherical symmetry in nanoparticles results in the introduction of anisotropy in the properties of the nanoparticles. In the context of plasmon vibration modes (the collective excitation of electrons) in such 'anisotropic' particles (that may be loosely quantified in terms of an aspect ratio parameter, defined as the ratio between the length of the nanoparticle and its cross-sectional dimension), an increase in the aspect ratio of silver and gold nanoparticles also leads to a shift in the in-plane surface plasmon absorption band to larger wavelengths that could be located well into the near infrared region (NIR) of the electromagnetic spectrum. This large absorption in the NIR region is expected to be of significance in cancer hyperthermia[13] and in the new cell imaging technique of plasmon resonance tomography.[14] Large aspect-ratio metal nanorods and nanowires are expected to play an important role in the electronics industry as interconnections in molecular circuits, as well as in the emerging area of plasmonics.[15]

In addition to anisotropic nanostructures, there is also considerable current interest in the synthesis of nanoscale structures consisting of a core of one chemical composition covered with a concentric shell of another material in what is commonly known as the 'core–shell' configuration. Insofar as bimetallic core–shell structures are concerned, studies have indicated that they have unique electronic and optical properties[16] distinct not only from the bulk metals but also from the corresponding monometallic nanoparticles. Interest in core–shell nanoparticles has centered on their potential application in areas such as biological labels,[17] optical resonance engineering,[18] catalysis,[19] magnetics[20] and in ceramics and pigments.[21] Coating of nanoparticles with materials of a different composition has also become an important route to functionalized nanomaterials. Such coatings not only stabilize nanoparticles but also allow their chemical modification and the tailoring of particle properties (*e.g.*, optical, magnetic, catalytic) depending on the coating composition.[22]

A special case of the core–shell nanostructure is that in which the core is empty, leading to hollow nanoparticles. Such hollow nanoparticles may be obtained by the synthesis of a core–shell structure followed by the subsequent removal of the core by either dissolution or decomposition.[23] The synthesis of hollow nanoparticles is exciting since these structures show increased surface area and low density, thus saving material and producing a concomitant reduction in cost, with potential application in catalysis[24] and cancer hyperthermia.[13] Hollow metallic nanoparticles may be prepared by coating the surface of latex particles, silica beads or gold and silver nanoparticles with the desired material and then etching away the core,[25] or by carrying out galvanic replacement reactions between sacrificial metal nanoparticles and suitable metal ions.[26]

In this article, we summarize our research efforts into the development of new experimental methods for the synthesis of anisotropic, core–shell and hollow metal nanoparticles. In section 2, we show how the spontaneous symmetry-breaking of the air–water interface may be used to generate anisotropic metal nanoparticles by localized reduction of metal ions at the interface. The synthesis of core–shell metal nanoparticles is normally accomplished by the reduction of the shell metal ions in the presence of the core nanoparticles. This procedure results in the formation of metal nanoparticles of the second metal in addition to the core–shell nanostructures and is clearly an undesirable aspect of the procedure. In section 3, we show that reducing agents bound to the surface of the core nanoparticle may be used to generate phase pure core–shell nanostructures. More specifically, we demonstrate how Keggin ions and the amino acid tyrosine bound to the surface of nanoparticles can be used as UV- and pH-switchable reducing agents, respectively, to synthesize phase pure core–shell nanoparticles. We end the article in section 4 with a description of the formation of hollow gold and platinum nanoparticles by a transmetallation reaction of hydrophobic silver nanoparticles with the corresponding metal ions in an organic medium.

2. Synthesis of anisotropic metal nanostructures at the air–water interface

The air–water interface has been widely used for the assembly of hydrophobized (water-insoluble) nanoparticles and, thereafter, the formation of multilayer films by the versatile Langmuir–Blodgett (LB) technique .[27] This procedure involves the dispersion of preformed hydrophobized nanoparticles in a volatile solvent, their organization at the air–water interface by spreading the dispersion on the surface of the water and then formation of mono/multilayer films of the nanoparticles onto suitable substrates by the vertical transfer LB technique. Apart from mere assembly, Fendler and co-workers have studied the synthesis of metal as well as semiconductor nanoparticles at the air–water interface in detail.[28] Their general strategy for the synthesis of metal nanoparticles involves spreading a Langmuir monolayer of suitable amphiphilic molecules over the surface of precursor ions in solution and then exposing the whole system to a suitable reducing environment. One handicap of this approach is that in addition to metal ion reduction at the air–water interface, reduction of ions also occurs in the

bulk of the subphase,[28] thereby making it difficult to ascertain the role played by the interface in determining particle morphology. In all previous studies on nanoparticle assembly and/or formation by chemical treatment of metal ions, the air–water interface is more or less passive and the built in anisotropy of the interface has not been utilized to its fullest extent. In this laboratory, we have recognized this lacuna and have designed two strategies that would lead to selective reduction of metal ions only at the air–water interface. These two approaches are based on: (1) confining the reducing species to the air–water interface by using an amphiphile in the Langmuir monolayer that both complexes and reduces metal ions from the subphase (Scheme 1a)[29a] and, (2) by confining the metal ions to be reduced to the air–water interface and having the reducing agent in the subphase (Scheme 1b).[29b] The highly interface-selective reduction of metal ions wherein the interface is a chemically active one results in highly anisotropic metal nanoparticles with interesting optical properties.

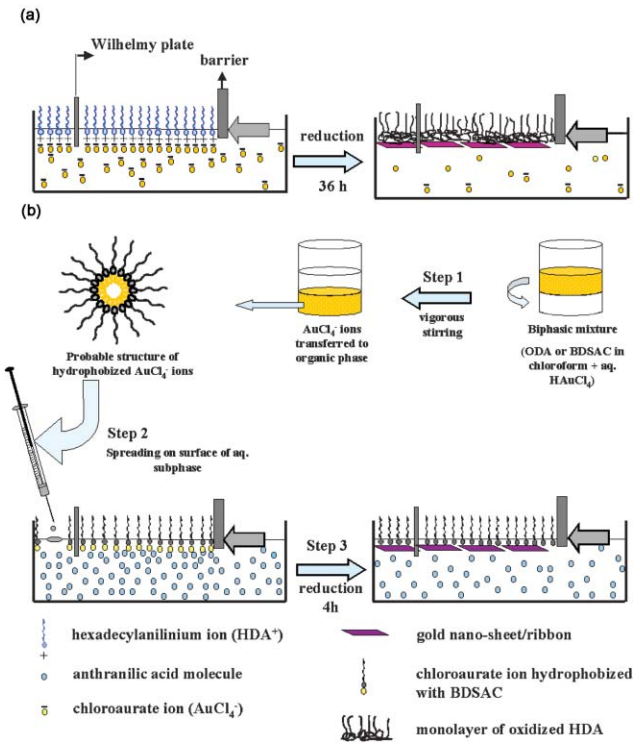

Scheme 1 (a) Diagram showing the formation of flat gold nanoribbons/nanosheets at the air–water interface by the spontaneous reduction of subphase chloroaurate ions by a 4-hexadecylaniline Langmuir monolayer. (b) Diagram showing the formation of gold nanostructures at the air–water interface by reduction of hydrophobized gold ions. Step 1: hydrophobization of chloroaurate ions by stirring the aqueous chloroauric acid solution with the solution of surfactants, ODA or BDSAC, in chloroform; step 2: immobilization of chloroaurate ions at the air–water interface by spreading the solution of hydrophobized chloroaurate ions on the surface of an aqueous anthranilic acid solution; step 3: formation of gold nanosheets by reduction of chloroaurate ions immobilized at the air–water interface by anthranilic acid in the subphase. (Adapted from ref. 29*b* © 2004 Royal Society of Chemistry.)

2.1 Langmuir monolayer as the metal ion complexing and reducing agent.

In this laboratory, the multifunctional capability of the molecule 4-hexadecylaniline (4-HDA) has been demonstrated for the one-step synthesis of gold[30a] and platinum nanoparticles[30b] in organic media. This molecule plays the role of a phase transfer agent (enabling transfer of aqueous $AuCl_4^-$/$PtCl_6^{2-}$ ions to an organic phase), reducing agent and capping agent, and leads to the formation of predominantly spherical nanoparticles of Au and Pt in the organic phase in a single step.[30] The Pt nanoparticles were shown to be catalytically active in spite of stabilization by the 4-HDA molecules.[30b] 4-HDA is a water-insoluble amphiphile and, thus, an excellent candidate for organization in the form of a Langmuir monolayer at the air–water interface. Making use of the built-in anisotropy of the air–water interface and the reducing capability of this amphiphile, we have shown that Langmuir monolayers of 4-HDA (conc.1 mg mL^{-1} in chloroform) organized on an aqueous subphase of 10^{-4} M chloroauric acid (pH *ca.* 3.2) results in the formation of nanosheets/ribbons of gold at the air–water interface (Scheme 1a).[29a] At this pH, the 4-HDA molecules are protonated and complex electrostatically with aqueous $AuCl_4^-$ ions, following which they are reduced by 4-HDA. Consequent to reduction, the 4-HDA Langmuir monolayer is oxidized, after which no further reduction of metal ions can occur. This process thus acts in a self-limiting fashion and restricts reduction of the gold ions to only those present in the vicinity of the interface.[29a]

The kinetics of reduction of gold ions at the air–water interface was followed by surface pressure–area (π–A) isotherm and transmission electron microscopy (TEM) measurements while LB films of the gold nanostructures on various substrates were characterized by X-ray diffraction (XRD) and UV-vis absorption spectroscopy. A series of π–A isotherms of the 4-HDA Langmuir monolayer, recorded as a function of time after spreading on the surface of the aqueous $HAuCl_4$ subphase, are shown in Fig. 1a (curves 1–6). A large expansion of the Langmuir monolayer with time is observed and is attributed to complexation and reduction of the gold ions by 4-HDA molecules and, thus, to the formation of gold nanostructures at the interface. TEM analysis of an LB film of these nanostructures after 36 h of reaction of the Langmuir monolayer with subphase gold ions indicated that they are extremely flat, ribbon-like structures with serrated edges (Fig. 2a and 2b). That the flat, gold nanosheets are single-crystalline in nature is indicated by the lattice planes corresponding to fcc gold, seen clearly in the high resolution TEM image of one of the nanostructures (Fig. 2c). That the gold nanosheets/ribbons are formed due to localized reduction of aqueous $AuCl_4^-$ ions by the 4-HDA Langmuir monolayer is indicated in a simple control experiment wherein the gold ions complexed with the 4-HDA Langmuir monolayer were rapidly reduced by exposure to hydrazine. The TEM image recorded from an LB film of the gold nanostructures obtained in this control experiment (Fig. 2d) shows that they are irregular in morphology and of much greater thickness than the structures for which 4-HDA was the reducing agent (Fig. 2a–c). Hydrazine is soluble in water and would lead to

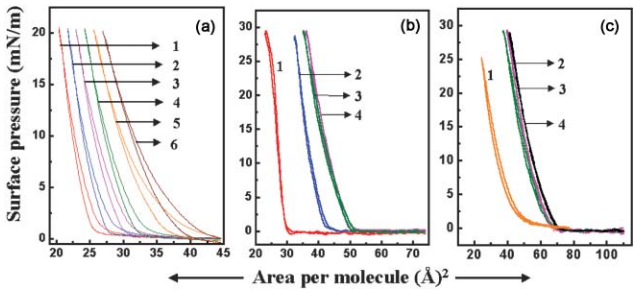

Fig. 1 (a) The π–A isotherms of a HDA Langmuir monolayer on the surface of aqueous 10^{-4} M chloroauric acid solution recorded as a function of time showing monolayer spreading; curves 1–6 correspond to the isotherms recorded at time, t = 15 min then 6, 12, 18, 24 and 36 h, respectively, after spreading the monolayer (adapted from ref. 29*a* © 2003 American Chemical Society); (b) curve 1: π–A isotherm during one compression and expansion cycle of ODA electrostatically complexed with chloroauric acid ($HAuCl_4$) on the acidic (pH 4.5) water subphase recorded 1 h after spreading the monolayer; curves 2, 3 and 4: π–A isotherms of ODA^+– $AuCl_4^-$ Langmuir monolayer on 10^{-4} M aqueous anthranilic acid subphase recorded 0, 1 and 3 h after spreading the monolayer, respectively; (c) curve 1: π–A isotherm during one compression and expansion cycle of benzyldimethylstearylammonium chloride (BDSAC) electrostatically complexed with chloroauric acid ($HAuCl_4$) on acidic (pH 4.5) water subphase recorded 1 h after spreading the monolayer; curves 2, 3 and 4: π–A isotherms of $BDSA^+$–$AuCl_4^-$ on 10^{-4} M aqueous anthranilic acid subphase recorded 0, 1 and 3 h after spreading the monolayer, respectively. (Reprinted with permission from ref. 29*b* © 2004 Royal Society of Chemistry.)

more delocalized reduction of the gold ions; this is not the case with 4-HDA Langmuir monolayer as reducing agent.

TEM kinetics study of the evolution of the gold nanostructures (Fig. 3a–d) confirmed that gold nanoribbons form mainly due to a templated growth process. One of the Interesting features of these nanostructures is that their growth is highly face selective. This is clearly illustrated by the presence of a highly intense (1 1 1) Bragg reflection in the XRD pattern of a 20-monolayer (20 ML) LB film of the gold nanoribbons transferred onto a glass substrate (Fig. 4a; the inset corresponds to a magnified view of the (2 0 0) and (2 2 0) Bragg reflection 2θ region).

In order to check whether formation of highly (1 1 1)-oriented, flat gold nanosheets/nanoribbons at the air–water interface is due to epitaxy between the 4-HDA Langmuir monolayer and the nucleating gold nanocrystals, efforts were made to break the periodicity of the 4-HDA Langmuir monolayer by mixing it with the surfactant, octadecylamine (ODA) in different ratios. The π–A isotherm measurements of mixtures of 4-HDA and ODA in molar ratios of 1 : 1 and 1 : 3 on an aqueous $HAuCl_4$ subphase did not show any evidence of phase separation and confirm the breakage in periodicity of the 4-HDA Langmuir monolayer. The XRD patterns of LB films of the gold nanostructures formed in these control experiments (formed from 4-HDA : ODA mixed Langmuir monolayers) also showed very strong (1 1 1) Bragg peaks indicating similar face-selective growth along the (1 1 1)-direction. These control experiments suggest that the formation of highly anisotropic, (1 1 1)-oriented gold nanostructures

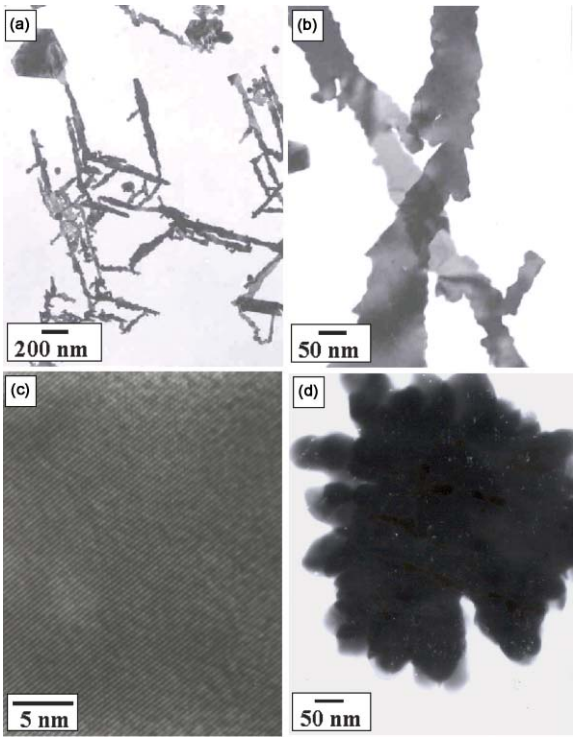

Fig. 2 (a–c) Representative TEM images at different magnifications of the LB film of gold nanosheets/ribbons formed by the reduction of chloroaurate ions in the subphase by the HDA Langmuir monolayer; (d) TEM image of a nanogold aggregate formed by hydrazine reduction of $AuCl_4^-$ ions complexed with HDA monolayer. (Reprinted with permission from ref. 29*a* © 2003 American Chemical Society.)

at the air–water interface is not a consequence of epitaxy with the 4-HDA Langmuir monolayer but most probably is due to surface energy considerations [the (1 1 1) crystallographic face of gold is the most energetically favorable crystal face] and stabilization of the nanosheets/nanoribbons by the oxidized product of 4-HDA. A useful characteristic of the anisotropic gold nanostructures grown at the air–water interface is that multilayer films of the nanoparticles of different thickness can be easily deposited on solid substrates in a layer-by-layer fashion by the LB technique. The growth of superlattices of the gold nanosheets/ribbons is indicated by the linear increase in intensity of gold surface plasmon absorption band centered at 610 nm as a function of number of monolayers in the LB film (UV-vis absorption spectra in Fig. 4b and inset). A large absorption in the near infrared (NIR) region of the electromagnetic spectrum is seen in LB films of the gold nanosheets/ribbons (Fig. 4b) and is a consequence of a red shift in the in-plane plasmon absorption of the anisotropic nanostructures. Aqueous spherical gold nanoparticles, on the other hand, show a sharp absorption at *ca.* 520 nm with negligible absorption beyond 600 nm.

2.2 Reduction of hydrophobized $AuCl_4^-$ ions by subphase anthranilic acid.

Khomutov and coworkers have shown the synthesis of Au and Pd nanoparticles at the air–water interface by spreading

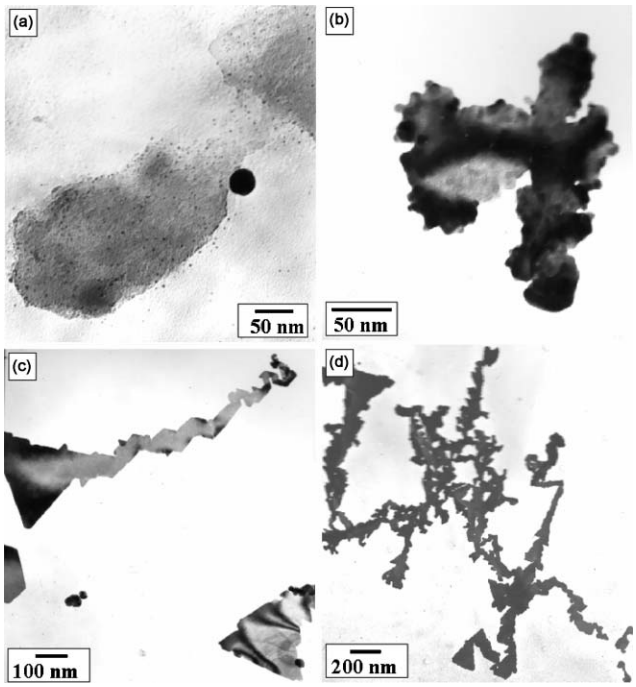

Fig. 3 (a–d) Representative TEM images recorded at time, t = 2, 6, 20 and 36 h respectively of formation gold nanosheets/ribbons by the reduction of chloroaurate ions in the subphase by the 4-HDA Langmuir monolayer. (Reprinted with permission from ref. 29*a* © 2003 American Chemical Society.)

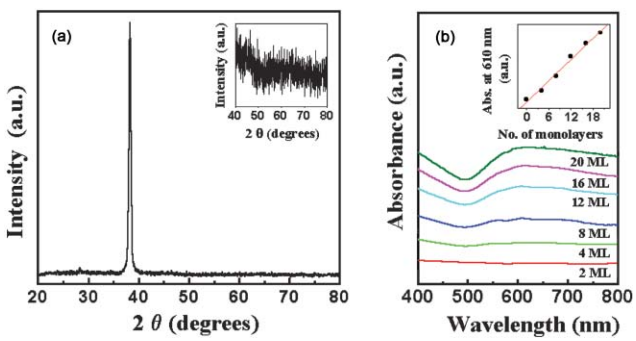

Fig. 4 (a) XRD pattern recorded from a 20 ML LB film of gold nanosheets/ribbons formed at the air–water interface deposited onto glass. The inset shows an expanded region of the XRD pattern highlighting the less intense Bragg reflections; (b) UV-vis absorption spectra recorded from LB films of the gold nanosheets/ribbons of different thickness (thickness in terms of number of monolayers is indicated next to the respective spectra) deposited on quartz. The inset shows the absorbance of gold nanoribbons at 610 nm plotted as a function of number of monolayers. (Reprinted with permission from ref. 29*a* © 2003 American Chemical Society.)

precursor organometallic complexes on the surface of an aqueous subphase containing a suitable reducing agent.[31] In this way, the metal ions were immobilized at the air–water interface along with a surfactant to slow down coalescence of the nuclei and to stabilize the nanoparticles against aggregation. Even after addition of surfactant, it was observed that aggregated, large spherical nanoparticles were formed possibly due to the phase separation of the precursor organometallic compounds from the surfactant molecules when spread on the surface of water.[31] In a different approach, that overcomes this problem of phase separation, we have used Langmuir monolayers of a single surfactant complexed with metal ions to confine the metal ions at the air–water interface.[29*b*] Thereafter, the metal ions immobilized at the air–water interface may be reduced by suitable reducing agents present in solution to yield anisotropic metal nanoparticles at the interface.

The basic ingredients of our recipe are illustrated in Scheme 1b. For the gold ions to be immobilized on the surface of water, they need to be rendered hydrophobic and this was accomplished by their phase transfer from the aqueous phase to chloroform using phase-transfer molecules such as octadecylamine (ODA) and benzyldimethylstearylammonium chloride (BDSAC, step 1, Scheme 1b). Spreading of hydrophobized $AuCl_4^-$ ions on the aqueous subphase, containing anthanilic acid as the reducing species, results in the formation of a uniform monolayer of gold ions on the surface of water with the metal ions complexed electrostatically with the surfactant (step 2). Reduction of the two dimensional assembly of gold ions by anthanilic acid results in the formation of gold nanostructures at the air–water interface (step 3). The π–A isotherm measurements of $AuCl_4^-$ ions complexed with ODA/BDSAC (Fig. 1b and 1c, respectively) confirmed that they form stable Langmuir monolayers on the surface of water as well as the aqueous anthranilic subphase. It is likely that once spread on the surface of water/aqueous anthranilic acid subphase, the micellar structure of the ODA^+–$AuCl_4^-$ and $BDSA^+$–$AuCl_4^-$ complexes is disrupted resulting in the formation of a gold ion–surfactant monolayer on the subphase (step 2). That the ODA/BDSAC Langmuir monolayers are stable in time is indicated by the control experiment wherein the monolayers were spread on water at a pH adjusted to 4.5 and the π-A isotherm recorded 1 h after spreading (curve 1 in Fig. 1b and 1c). An expansion in the ODA/BDSAC monolayer on anthanilic acid solution with time is seen that stabilizes 3 h after spreading the monolayer in each case (Fig. 1b and 1c, curves 2–4). This indicates that the gold ion reduction is complete within this time interval. The process of reduction of the gold ions by anthranilic acid in the subphase could be observed by the appearance of a faint violet color at the interface that is characteristic of gold nanostructures.

The morphology of anthranilic acid-reduced gold nanostructures formed at the air–water interface was studied by depositing a one monolayer (1 ML) LB film of the nanoparticles on carbon-coated TEM grids. Fig. 5a–d, 6a and 6b show representative TEM images of anthranilic acid-reduced gold nanoparticles obtained from the ODA^+–$AuCl_4^-$ and $BDSA^+$–$AuCl_4^-$ Langmuir monolayers, respectively, at different magnifications. An important and fascinating feature of the gold nanostructures obtained by reduction of the ODA^+–$AuCl_4^-$ monolayer is that they show a high frequency of fractal, dendritic structures of nanoscale dimensions extending to lengths of up to 200 nm (Fig. 5a–d). Fractal dimensions of a number of nanostructures in these images were calculated and were observed to vary from 1.71 $\pm$ 0.2 to 1.8 $\pm$ 0.1. The gold fractal nanostructures obtained in this study are characteristic of diffusion-limited aggregated (DLA) structures.[32] The formation of fractal gold nanostructures by the spontaneous

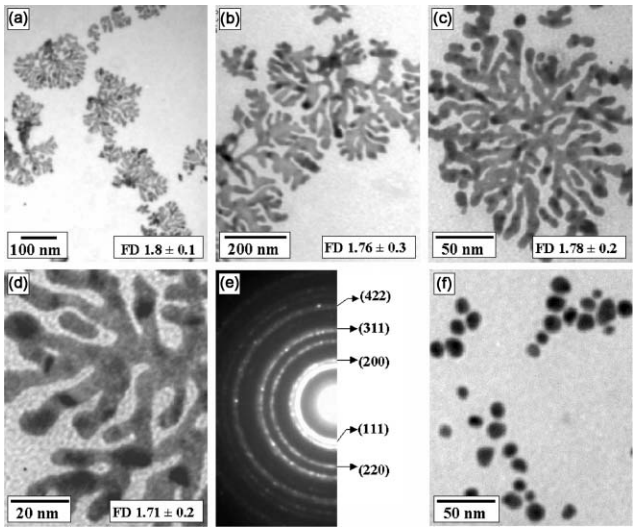

Fig. 5 (a–d) Representative TEM images of gold nanostructures formed at the air–water interface by the reduction of $AuCl_4^-$ ions (immobilized on the surface of 10^{-4} M aqueous anthranilic acid subphase by complexing with ODA) using anthranilic acid as a reducing agent present in the subphase, recorded at different magnifications. The respective fractal dimensions are shown in the images; (e) electron diffraction pattern recorded from the flat gold nanostructures shown in image (d); (f) TEM image of gold nanoparticles formed at the liquid–liquid interface by the reduction of hydrophobized $AuCl_4^-$ ions (hydrophobized by complexing with ODA) in chloroform using 10^{-3} M aqueous anthranilic acid solution as a reducing agent present in the biphasic mixture. (Reprinted with permission from ref. 29*b* © 2004 Royal Society of Chemistry.)

reduction of chloroaurate ions entrapped in thermally evaporated hexadecylaniline thin films due to diffusion limited aggregation has also been demonstrated in this laboratory.[33] We believe that the strong binding of the ODA molecules with the gold nanoparticle surface (since chloroaurate ions are hydrophobized with ODA before spreading on surface of aqueous subphase) may be partly responsible for this observation. While irregular, flat gold nanosheets of size ranging from 10 to 100 nm were obtained by reduction of the $BDSA^+$–$AuCl_4^-$ monolayer at the air–water interface (Fig. 6a and 6b), they did not demonstrate the same fractal structure observed in the case of the ODA^+–$AuCl_4^-$ monolayer. Selected area electron diffraction (SAED) patterns recorded from the single flat gold nanostructures obtained using ODA and BDSAC as the gold ion immobilizing agents (Fig. 5e and inset Fig. 6a, respectively) clearly show that they are polycrystalline in nature. A control experiment was performed wherein $AuCl_4^-$ ions, hydrophobized with ODA and BDSAC in chloroform, were reduced separately at the liquid–liquid interface using 10^{-3} M aqueous anthranilic acid solution under constant stirring for 1 h. This resulted in the formation of spherical gold particles of size 10–20 nm (Fig. 5f and 6c for ODA and BDSAC, respectively), quite different in morphology from the flat, anisotropic structures obtained at the air–water interface. The TEM images indicate that the formation of anisotropic gold nanostructures at the air–water interface is really a consequence of localization of gold ions at the two dimensional surface.

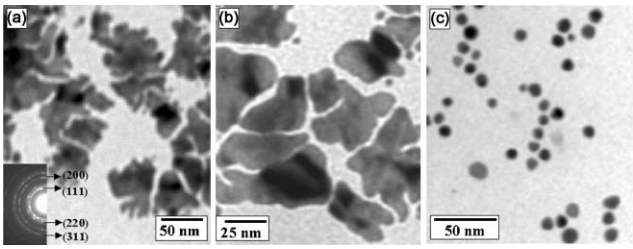

Fig. 6 (a, b) Representative TEM images of gold nanostructures formed at the air–water interface by the reduction of $AuCl_4^-$ ions (immobilized on the surface of 10^{-4} M aqueous anthranilic acid subphase by complexing with BDSAC) using anthranilic acid as a reducing agent present in the subphase, recorded at different magnifications. The inset in (a) shows the SAED pattern recorded from the nanosheets in the main part of the figure; (c) TEM image of the gold nanoparticles formed at the liquid–liquid interface by the reduction of hydrophobized $AuCl_4^-$ ions (hydrophobized by complexing with BDSAC) in chloroform using 10^{-3} M aqueous anthranilic acid solution as a reducing agent present in the biphasic mixture. (Adapted from ref. 29*b* © 2004 Royal Society of Chemistry.)

It is observed that the dimensions of the gold nanostructures formed in the present study (50–200 nm) are much smaller than the gold nanoribbons that extended up to a few micrometers in length by the reduction of $AuCl_4^-$ ions using 4-HDA Langmuir monolayer as a reducing agent (Fig. 2a). We believe this is due to the low concentration of $AuCl_4^-$ ions within the Langmuir monolayer of ODA^+–$AuCl_4^-$ and $BDSA^+$–$AuCl_4^-$ in comparison with the comparatively high concentration at the interface when the 4-HDA monolayer was spread on the aqueous $HAuCl_4$ subphase. UV-vis absorption spectra of LB films of different thickness of the gold nanostructures obtained by the reduction of ODA^+–$AuCl_4^-$ and $BDSA^+$–$AuCl_4^-$ monolayers (Fig. 7a and 7b, respectively) show broad absorption bands centered at *ca.* 565 nm and 590 nm, respectively, that are due to the excitation of surface plasmon vibrations in the particles. The intensity of the absorption at these wavelengths increases linearly with increasing number of monolayers in the LB films formed from ODA and BDSAC (insets of Fig. 7a and b) indicating that good quality superlattices of the particles can conveniently be deposited by the LB technique. The shift and broadening of the plasmon band from the gold nanoparticles in the LB films indicates anisotropy in shape of the particles and is well supported by the TEM results (Fig. 5 and 6).

3. Synthesis of metallic core–shell nanoparticles

Two main groups of bimetallic nanoparticles exist, *viz.* alloys and layered (core–shell) structures. Bimetallic nanoparticles can be prepared by the simultaneous co-reduction of two kinds of metal ions with or without a protective agent (usually a polymer or a surfactant)[34] or by successive reduction of one metal over the nuclei of another.[35] The preparation and characterization of bimetallic nanoparticles from various combinations of noble metals has been the subject of numerous papers, examples of which include the Au–Pd,[36] Au–Pt,[37] Ag–Pd,[38] Ag–Pt,[39] and Ag–Au[40] systems. Up to now, many routes have been explored to fabricate core–shell

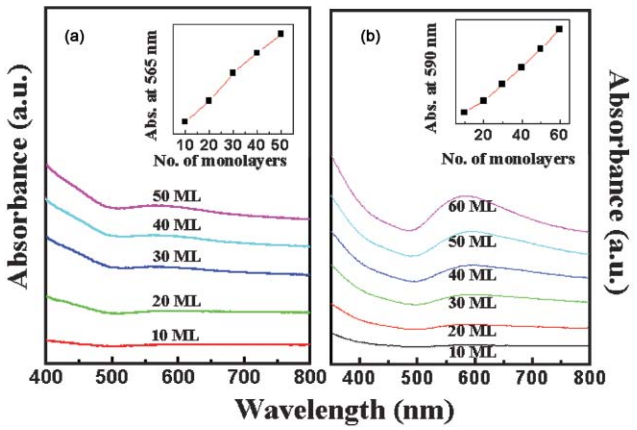

Fig. 7 UV-vis absorption spectra of LB films of gold nanoparticles deposited on a quartz substrate formed at the air–water interface by the reduction of chloroaurate ($AuCl_4^-$) ions (immobilized at air–water interface) using 10^{-4} M anthranilic acid as a reducing agent present in the subphase, recorded as a function of number of monolayers in the LB films; (a) $AuCl_4^-$ ions immobilized at the air–water interface using octadecylamine, ODA. The inset is a plot of intensity of the surface plasmon resonance (absorbance at 565 nm) as a function of number of monolayers in the LB films; (b) $AuCl_4^-$ ions immobilized at the air–water interface using benzyldimethylstearylammonium chloride, BDSAC. The inset shows a plot of intensity of the surface plasmon resonance (absorbance at 590 nm) plotted as a function of number of monolayers in the LB films. The number of monolayers of gold nanoparticles in the LB films in both cases is indicated next to the respective curves. (Adapted from ref. 29*b* © 2004 Royal Society of Chemistry.)

particles, such as electroless plating,[41] surface precipitation reaction,[42,43] surface seeding,[44] and self-assembly.[45] However, in most cases, the degree of surface coverage is low and the metallic coating is nonuniform and, consequently, the preparation of a composite particle with uniform and complete metallic nanoshell coverage remains a challenge. Generally, core–shell nanoparticles are prepared by the successive reduction of one metal ion over the core of another.[46] This process often leads to the formation of fresh nuclei of the second metal in solution, in addition to a shell around the first metal core,[46] and is clearly undesirable from an application point of view. We have developed a strategy to overcome this drawback by immobilization of a reducing agent on the surface of the core metal which, when exposed to the second metal ions, reduces them, thereby leading to the formation of a thin metallic shell.[47] The surface bound reducing agents investigated in this laboratory are Keggin ions (UV-switchable reducing agent) and the amino acid tyrosine (pH dependent reducing agent) and have been successfully used in the synthesis of phase pure core–shell metallic nanoparticles.

3.1 Keggin ions as UV-switchable reducing agent.

It is well known that polyoxometalates such as Keggin ions undergo stepwise multielectron redox processes without undergoing a structural change.[48] They may be reduced electrolytically, photochemically and with suitable reducing agents. Photochemically-reduced polyoxometalates of the Keggin structure [$(PW_{12}O_{40})^{3-}$ and $(SiW_{12}O_{40})^{4-}$] when exposed to aqueous metal ions such as Ag^+, $AuCl_4^-$, Pd^{2+} and $PtCl_6^{2-}$ have been shown to result in the formation of stable metal nanoparticles capped by the Keggin ions.[49] We realized that in addition to being an excellent capping and stabilizing agent for the nanoparticles, surface-bound Keggin ions may be UV-excited and thereafter, used as highly localized reducing agents for the formation of thin shells of another metal. The entire process is illustrated in the schematic shown in Fig. 8a. In a typical experiment 30 mL of 10^{-2} M aqueous deaerated solution of phosphotungstic acid (PTA) was added to 2 mL of propan-2-ol, and the mixture was irradiated by UV light for 4 h (Pyrex filter, >280 nm, 450 W Hanovia medium-pressure lamp, step 1). This leads to reduction of $(PW_{12}O_{40})^{3-}$ ions and is seen as a blue color appearing in the solution (sample bottle 1, inset of Fig. 8b). The UV-vis absorption spectrum recorded from the UV-irradiated Keggin ion solution is shown as curve 1 in Fig. 8b, 9a and 9b. The blue color in this solution arises from the strong absorption band at 760 nm that is characteristic of one-electron reduced PTA, $[PW_{12}O_{40}]^{4-}$.[48] To 5 mL of this irradiated PTA solution, 15 mL of 10^{-3} M $HAuCl_4$ solution was added under continuous stirring for 10 min, and then the solution was allowed to age for 2 h (step 2). The solution changed color from blue to pink indicating formation of gold nanoparticles (sample bottle 2, inset of Fig. 8b). The UV-vis absorption spectrum recorded from this solution is shown as curve 2 in Fig. 8b, 9a and 9b. It is seen that the peak at 760 nm characteristic of reduced PTA ions is now almost of negligible intensity while a strong absorption at *ca.* 526 nm due to surface plasmon excitation in the gold nanoparticles appears.[50] Uncoordinated PTA ions in solution were removed by thoroughly dialyzing the PTA-gold nanoparticle solution against distilled water for 2 days, using a 12 K cutoff dialysis bag. The dialyzed solution was also extremely stable over time and indicated that the Keggin ions are bound to the nanoparticle surface and stabilizes it electrostatically and stereochemically. Following dialysis of the

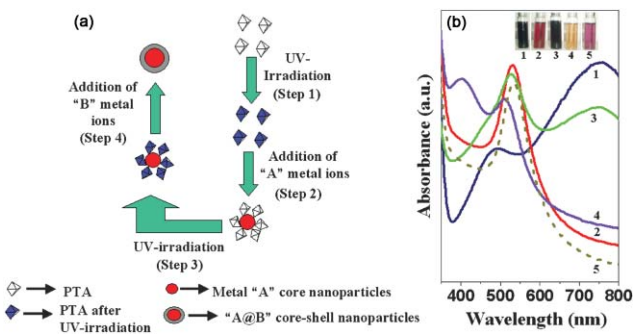

Fig. 8 (a) Scheme of the Keggin ion-mediated synthesis of Au core–Ag shell nanoparticles. For simplicity, Keggin ions are shown as octahedral particles; (b) UV-vis absorption spectra recorded from: (1) 10^{-2} M aqueous solution of PTA after UV irradiation; (2) UV-irradiated PTA solution after addition of 10^{-3} M $HAuCl_4$; (3) solution 2 after further UV irradiation; (4) solution 3 after addition of 10^{-3} M Ag_2SO_4 solution; and (5) solution 2 after addition of 10^{-3} M Ag_2SO_4. All UV-vis spectra have been adjusted for solution dilution effects. Pictures of sample bottles containing solutions 1–5 are shown in the inset. (Reprinted with permission from ref. 47*a* © 2003 American Chemical Society.)

PTA-gold nanoparticle solution, it was UV-irradiated again for 4 h (step 3) as a consequence of which the solution color changed from pink to a bluish-red (sample bottle 3, inset of Fig. 8b). The UV-vis absorption spectrum from this solution (curve 3 in Fig. 8b, 9a and 9b) shows an additional band at longer wavelengths that is characteristic of reduced PTA ions now bound to the surface of the gold nanoparticles. To 15 mL each of this solution, 15 mL aqueous solutions of 10^{-3} M Ag_2SO_4, 10^{-4} M $Pd(NO_3)_2$ and 10^{-4} M chloroplatinic acid (H_2PtCl_6) were added separately under stirring conditions (step 4). In the case of reaction with Ag^+ ions, the solution color rapidly turned to a pale yellowish brown indicating formation of silver nanoparticles (sample bottle 4, inset of Fig. 8b). The absorption band at *ca.* 415 nm that appears after this reaction is due to excitation of surface plasmon vibrations in the silver nanoparticles (curve 4, Fig. 8b) and is responsible for this color. In the case of reaction of UV-excited Keggin ion capped gold nanoparticles with $Pd(NO_3)_2$ and H_2PtCl_6, changes in solution color are not so dramatic since nanoparticles of Pd and Pt do not absorb strongly in the visible region of the electromagnetic spectrum. Nevertheless, that reduction of Pd and Pt ions has taken place is indicated by a dampening of the surface plasmon band of the gold core (curve 4 in Fig. 9a and 9b, respectively), a feature also observed for the gold nanoparticles capped with a silver shell (curve 4, Fig. 8b). These observations are symptomatic of formation of silver/Pd/Pt shells around the PTA-capped gold nuclei (step 4 in Fig. 8a) and are consistent with previous observations that the presence of a group 10 metal (d^8s^2) in bimetallic nanoparticles suppresses the surface plasmon energies of the group 11 core metal ($d^{10}s^1$).[51]

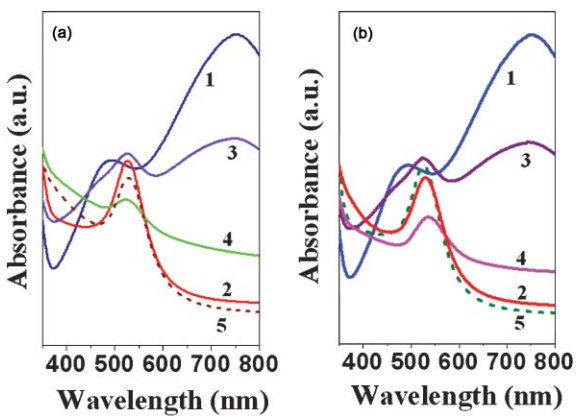

Fig. 9 (a, b) UV-vis absorption spectra of the Au core–Pt/Pd shell nanoparticle solutions, respectively, at different stages of the reaction; curve 1 in (a) and (b): 10^{-2} M aqueous solution of PTA after UV irradiation; curve 2 in (a) and (b): UV-irradiated PTA solution after addition of 10^{-3} M $HAuCl_4$; curve 3 in (a) and (b): PTA-capped Au nanoparticle solution after further UV irradiation; curve 4 in (a) and (b): UV irradiated PTA-capped Au nanoparticle solution after addition of 10^{-4} M aqueous solutions of $Pd(NO_3)_2$ and H_2PtCl_6 respectively and curve 5 in (a) and (b): PTA-capped Au nanoparticle solution shown as curve 2 after addition of 10^{-4} M $Pd(NO_3)_2$ and H_2PtCl_6 solutions respectively (without prior UV-irradiation, see text for details). (Reprinted with permission from ref. 47*b* © 2004 Royal Society of Chemistry.)

Fig. 10a shows a representative low-magnification TEM image of PTA-capped Au nanoparticles. The nanoparticles are polydisperse (sizes ranging from 15 to 50 nm) and have irregular morphology. Fig. 10b shows a high-resolution TEM image of a few gold nanoparticles. A number of multiply twinned gold nanoparticles are observed, which at higher magnification clearly showed the lattice planes of fcc gold. Fig. 10c shows a representative TEM picture of a drop-cast film of Au core–Ag shell nanoparticles formed using Keggin ions. The particles are quite polydisperse, show a small increase in size (ranging from 20 to 100 nm), and are of varying morphology. To confirm formation of core–shell nanoparticle structures, high resolution TEM is one of the most important tools. A representative HRTEM image of one Au core–Ag shell nanoparticle is shown in Fig. 10d. A distinct variation in contrast between the dark gold core and the lighter silver shell is clearly seen. The thickness of the shells varied across particles and often exhibited morphology different from that of the core. Fig. 11a and b show representative low and HRTEM pictures of a drop-cast film of Au core-Pd shell nanoparticles grown as described above. A distinct variation in contrast between the dark gold core and the lighter palladium shell is clearly seen in Fig. 11b. The moiré fringes observed in the particles (Fig. 11b) suggest that they are composed of a superposition of two crystallites that have very similar crystal structure. Fig. 11c and d show representative low and high-resolution TEM pictures of a drop-cast film of Au core–Pt shell nanoparticles. An increase in particle size is observed after formation of the Pt shell and the contrast between the Au core and Pt shell is clearly seen (Fig. 11c). The lattice fringes from the Pt shell are clearly seen in HRTEM image of Fig. 11d, which clearly indicates the crystalline nature of the bimetallic nanoparticles.

From the above, discussion it is clear that, after UV-irradiation, surface bound PTA molecules on Au-core

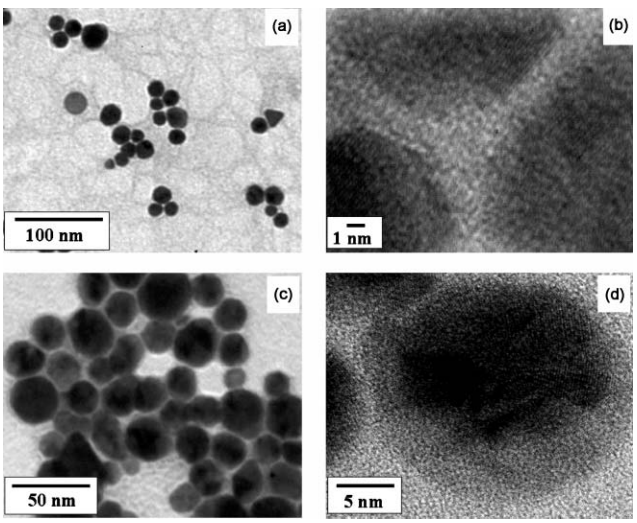

Fig. 10 (a) TEM picture of PTA-capped gold nanoparticles; (b) high resolution TEM image of the gold particles; (c, d): low and high-resolution TEM images recorded from gold core–silver shell nanoparticles. (Adapted from ref. 47*b* © 2004 Royal Society of Chemistry and ref. 47*a* © 2003 American Chemical Society.)

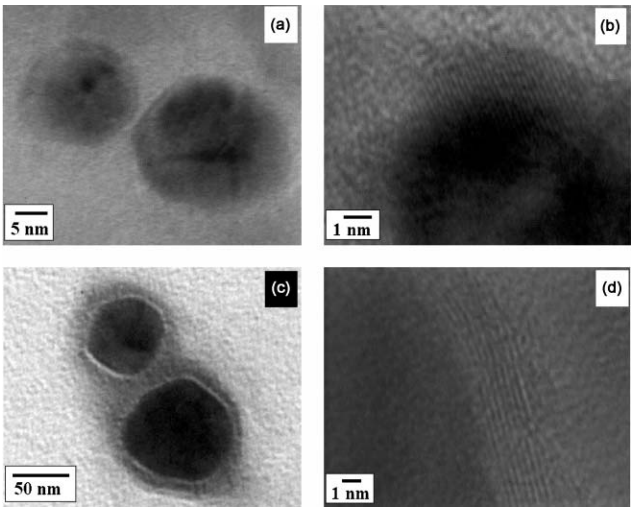

Fig. 11 (a, b) Low and high-resolution TEM images recorded from gold core–palladium shell nanoparticles; (c) TEM picture of gold core–platinum shell nanoparticles by sequential reduction of gold and platinum ions by UV-irradiated PTA solution; (d) high-resolution TEM image of one of the Au core–Pt shell nanoparticles. (Reprinted with permission from ref. 47*b* © 2004 Royal Society of Chemistry.)

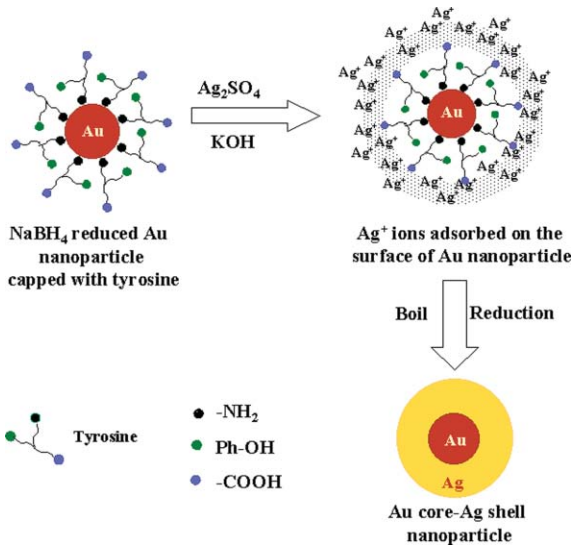

Scheme 2 Formation of Au core–Ag shell nanoparticles using amino acid tyrosine as pH dependable reducing agent. (Adapted from ref. 47*c* © 2004 American Chemical Society.)

nanoparticles act as a highly localized reducing agent for Ag, Pd and Pt metal ions. Is it really necessary to photochemically charge the surface bound PTA molecules to reduce the Ag, Pd and Pt metal ions? To answer this question, control experiments were performed wherein Ag^+, Pd^{2+} and Pt^{4+} ions were added separately to PTA-capped gold nanoparticle solutions without additional UV irradiation. Little change in the solution colors occurred and were supported by negligible changes in the solution UV-vis absorption spectra recorded before (curve 2 in Fig. 8b, 9a and 9b) and after ion exposure (curve 5 in Fig. 8b, 9a and 9b). Thus, photochemical charging of PTA molecules bound to the gold nanoparticle surface is a crucial step in this work, that sets it apart from other bimetallic nanoparticle core–shell synthesis protocols that employ reducing agents uniformly present in the reaction medium. That the reducing capability of the Keggin ions can be switched on using UV irradiation, is an additional feature that enhances the versatility of the technique.

3.2 Tyrosine as pH dependent reducing agent.

The amino acid tyrosine is capable of reducing silver ions under alkaline conditions to yield highly stable silver nanoparticles, but not under neutral and acidic conditions.[47c] This reducing ability of tyrosine at alkaline pH is due to the ionization of the phenolic group in the amino acid to phenolate ions, which thereafter reduce the silver ions, by electron transfer, into silver nanoparticles. The pH-dependent reducing capability of tyrosine has been used in the synthesis of Au core–Ag shell nanoparticles by first capping gold nanoparticles with tyrosine and then using the surface bound tyrosine molecules to reduce silver ions under alkaline conditions to yield gold core–silver shell bimetallic structures (Scheme 2). It may be immediately recognized that since the reducing agent tyrosine is bound to the surface of the gold nanoparticles and is not present in solution, silver ion reduction takes place only on the gold surface, thus avoiding nucleation and growth of silver nanoparticles in solution.

In a typical experiment, a 10^{-4} M aqueous solution (100 mL) of chloroauric acid ($HAuCl_4$) was reduced by 0.01 g of sodium borohydride ($NaBH_4$) at room temperature. This procedure results in a ruby-red solution containing gold nanoparticles of dimensions 35 $\pm$ 7 Å (solution pH *ca.* 9.5).[52] The gold nanoparticles were capped with tyrosine by addition of 10 mL aqueous solution of 10^{-3} M tyrosine to 90 mL of the gold nanoparticle solution and were allowed to age for 1 day. This solution was dialyzed using a semipermeable membrane to remove excess uncoordinated tyrosine molecules. To 90 mL of the dialyzed tyrosine-capped gold nanoparticle solution, 10 mL of 10^{-3} M Ag_2SO_4 and 1 mL of 10^{-1} M KOH solution were added, and the solution was allowed to boil until its color changed from purple to brownish yellow (Au/Ag core shell 1). To vary the thickness of the silver shell over the tyrosine-capped gold nanoparticles, 5 mL of 10^{-3} M silver sulfate solution was added to 95 mL of dialyzed tyrosine-capped gold nanoparticle solution and allowed to boil until completion of the reaction (Au/Ag core shell 2).

Fig. 12a shows the UV-vis absorption spectra recorded from the tyrosine-capped gold nanoparticles before (Fig. 12a, curve 1) and after addition of KOH (curve 2) and after reaction with aqueous silver ions at concentrations of 10^{-4} M (curve 4) and 5 $\times$ 10^{-5} M (curve 3). While the optical properties of the tyrosine-capped gold nanoparticles do not change significantly after addition of KOH (curves 1 and 2), reaction of the amino acid capped gold nanoparticles with Ag^+ ions does lead to large changes in the absorption spectra (compare curve 1 with curves 3 and 4). The common feature in the spectra of curves 3 and 4 after reaction of the tyrosine-capped gold nanoparticles with silver ions is the appearance of an absorption band centered at *ca.* 405 nm in addition to the plasmon vibration band of gold nanoparticles at 520 nm. The

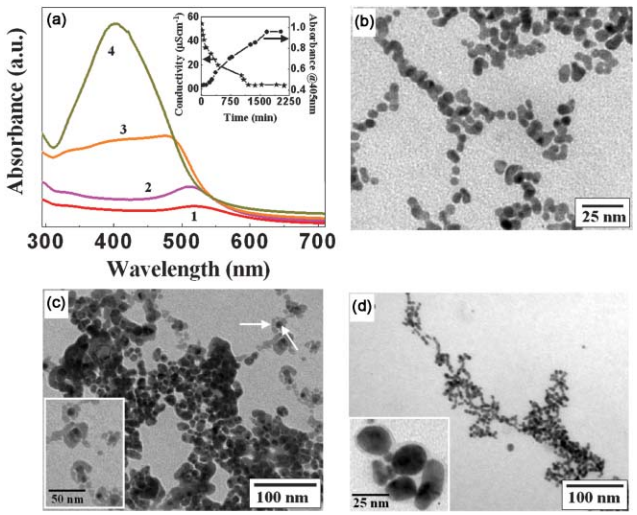

Fig. 12 (a) UV-visible spectra recorded from tyrosine-capped gold nanoparticles (curve 1); the tyrosine-capped gold nanoparticle solution after addition of KOH (curve 2); Au core–Ag shell bimetallic nanoparticles synthesized wherein the silver ion concentration in solution is 5×10^{-5} M (curve 3) and 10^{-4} M (curve 4). The inset in (a) shows the absorbance values at 405 nm from the UV-vis absorption spectra plotted against time during the silver shell formation on the surface of tyrosine-capped gold nanoparticles (circles, right axis) and the solution conductivity data (stars, left axis); (b) representative TEM image of tyrosine-capped gold nanoparticles after dialysis; (c, d) representative TEM images of Au core–Ag shell nanoparticles synthesized under conditions where the silver ion concentration in solution was 10^{-4} and 5×10^{-5} M, respectively. The insets in (c) and (d) show magnified regions of the core–shell nanoparticles for clarity. (Adapted from ref. 47*c* © 2004 American Chemical Society.)

resonance at 405 nm is due to excitation of surface plasmon vibrations in silver nanoparticles[53] that are formed after the reduction of Ag^+ ions by the ionized tyrosine molecules present on the gold nanoparticle surface. For smaller amounts of Ag^+ ions in the reaction medium (curve 3, 5×10^{-5} M silver ions), the damping of the gold plasmon band and intensity of the silver plasmon band are less than those observed for the 10^{-4} M Ag^+ ion reaction case (curve 4). Since the tyrosine is bound to the surface of the gold nanoparticles (note that uncoordinated tyrosine was removed by dialysis of the gold nanoparticle solution), reduction of the silver ions is expected to occur only on the surface of the gold particles, leading to an Au core–Ag shell bimetallic structure (Scheme 2). The possibility of alloy formation may be ruled out since, in such cases, a single surface plasmon band is expected, the position of which would depend on the relative concentration of gold : silver in the alloy.[50,54] The kinetics of formation of the silver shell around the gold core in the 10^{-4} M Ag^+ ion reaction was followed by UV-vis absorption spectroscopy (spectra not shown for brevity), and the absorption at 405 nm (due to the silver shell) was plotted against time (inset of Fig. 12a, circles, right axis). During this reaction, the conductivity of the reaction solution was also monitored (inset of Fig. 12a; stars, left axis). Immediately after addition of silver ions to the tyrosine-capped gold nanoparticle solution at pH 10, it is seen that the plasmon resonance intensity increases rapidly and is accompanied by a large fall in solution conductivity, both of which indicate reduction of the metal ions to metallic silver. After *ca.* 24 h of reaction, the conductivity and plasmon absorption intensity achieve saturation indicating completion of the reduction of silver ions. Thus, the surface reduction of the Ag^+ ions by tyrosine is fairly slow. It is interesting to note the faithful tracking of the solution conductivity with increase in the silver nanoshell plasmon intensity (inset in Fig. 12a).

Fig. 12b shows a representative TEM image recorded from the tyrosine-capped gold nanoparticles after dialysis of the solution for 1 day. The gold particles are fairly spherical (6 nm average size) and are assembled into quasi-linear superstructures, presumably by hydrogen bonding between the tyrosine molecules bound to the gold nanoparticles.[55] After addition of silver ions to the solution, it was observed that the solution color turned rapidly to light blue, suggesting Ag^+ ion-induced aggregation of the tyrosine-capped gold nanoparticles. During heating of the Ag^+–tyrosine-capped gold nanoparticle solution, it was observed that the blue color disappeared and that the solution attained a pale yellow color indicative of formation of nanoparticles of metallic silver. Representative TEM images of the tyrosine-capped gold nanoparticles after reaction with aqueous solutions of 10^{-4} and 5×10^{-5} M Ag^+ ions are shown in Fig. 12c and 12d, respectively. The formation of a silver shell around the gold core is seen in many of the nanoparticles as a "halo" around a dark core. One of the particles showing this effect very clearly is identified by arrows in Fig. 12c and the magnified region has been shown in inset of the main figure. While the halo could be observed in the case of the 10^{-4} M experiment, it was not so evident in the case of core–shell structures formed in the 5×10^{-5} M case (inset of Fig. 12d). In this experiment, we see that the gold nanoparticles are aligned in a chainlike superstructure. Binding tyrosine to the surface of gold nanoparticles through the amine groups in the amino acid thus provides a versatile means of selectively reducing silver ions on the surface of the gold nanoparticles at alkaline pH to yield phase-pure Au core–Ag shell nanostructures.

4. Organic phase synthesis of hollow Au and Pt nanoparticles by transmetallation reaction

Hollow (shell) nanostructures have received considerable attention due to their application in drug delivery,[56] thermal therapy of tumors[57] and catalysis.[58] The Bai[24] and Xia[59] groups have recently demonstrated a promising route to obtaining water-dispersible hollow metal nanostructures of various shapes by a simple transmetallation reaction. This elegant method employs a sacrificial nanoparticle that, by a galvanic replacement reaction with another suitable metal ion (transmetallation reaction), results in the formation of excellent hollow particles that take on the morphology of the sacrificial partner.[24,59] Recently we have shown that a similar transmetallation reaction involving hydrophobic spherical silver nanoparticles and hydrophobized $AuCl_4^-$ and $PtCl_6^{2-}$ ions may be carried out in an equally facile manner in organic solvents resulting in excellent Au and Pt nanoparticles with hollow interior that are organically dispersible.[60]

Silver nanoparticles synthesized in water by sodium borohydride reduction of silver sulfate ions were immediately transferred into chloroform by stirring with 10^{-3} M chloroform solution of octadecylamine (ODA).[53b] After the complete transfer of silver nanoparticles into the organic medium, it was separated from the aqueous phase and purified as described elsewhere.[53b] Phase transfer of aqueous chloroaurate ions was achieved by the vigorous stirring of aqueous chloroauric acid with 10^{-3} M chloroform solution of octadecylamine (ODA).[29b] Aqueous chloroplatinate ions ($PtCl_6^{2-}$) ions were phase transferred into chloroform in a similar manner but benzyldimethylstearylammonium chloride (BDSAC) was used as the metal ion phase transfer molecule instead of ODA. The appearance of a yellow color in the chloroform phase indicated the transfer of chloroaurate and chloroplatinate ions and assuming complete transfer of these ions to the chloroform phase,[29b] the concentration of these ions was calculated to be 10^{-3} M. The hydrophobized chloroaurate and chloroplatinate ions were separated from the aqueous phase and used as such for further experiments. Different volumes of 10^{-3} M hydrophobized $AuCl_4^-$ ions in chloroform were added to 19 ml of the ODA-capped Ag nanoparticles in chloroform to yield 3×10^{-5}, 5×10^{-5}, 10^{-4} and 5×10^{-4} M of $AuCl_4^-$ ions in the reaction medium. In almost all cases, the solution rapidly changed color from yellow (test tube 1, inset of Fig. 13a) to different shades of red/pink (test tube 2, Fig. 13a) indicating reduction of gold ions and oxidation of silver atoms. Curve 1 in Fig. 13a corresponds to the UV-vis absorption spectrum of the ODA-capped Ag nanoparticles in chloroform; the strong absorption at 410 nm is due to excitation of surface plasmon vibrations in the nanoparticles. Fig. 14a shows a TEM picture of the ODA-capped silver nanoparticles drop-coated from

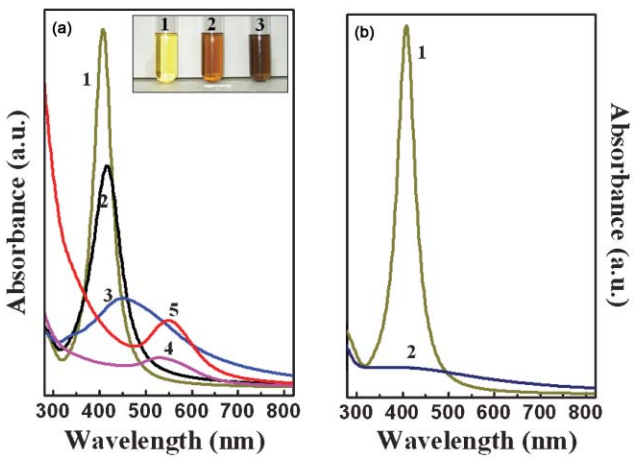

Fig. 13 (a) UV-vis absorption spectra recorded from ODA-capped Ag nanoparticles in chloroform at various stages of reaction; 1: as-prepared ODA-capped silver nanoparticles; 2 to 5: after addition of 3×10^{-5}, 5×10^{-5}, 10^{-4} and 4×10^{-4} M of hydrophobized $AuCl_4^-$ ions, respectively. The inset shows pictures of the ODA-capped silver nanoparticles in chloroform before (1) and after addition of hydrophobized $AuCl_4^-$ (2) and $PtCl_6^{2-}$ ions (3); (b) UV-vis absorption spectra recorded from ODA-capped silver nanoparticles in chloroform before (1) and after addition of 5×10^{-5} M of hydrophobized $PtCl_6^{2-}$ ions (2). (Reprinted with permission from ref. 60 © 2005 Royal Society of Chemistry.)

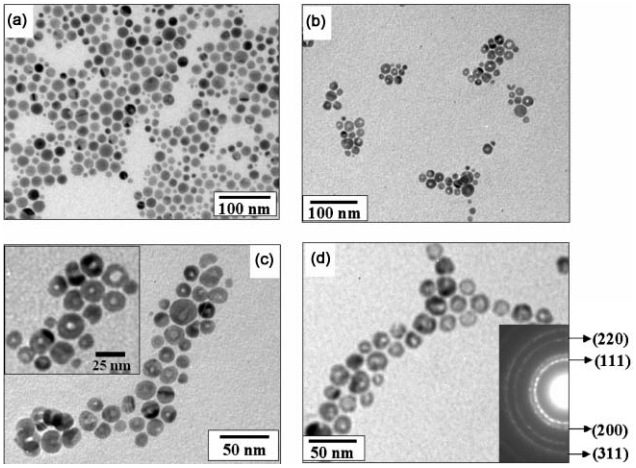

Fig. 14 (a) Representative TEM picture of ODA-capped Ag nanoparticles in chloroform; (b and c, inset in c) representative TEM images, at different magnifications, of hollow Au nanoparticles obtained by reaction of ODA-capped Ag nanoparticles with hydrophobized $AuCl_4^-$ ions; (d) hollow Pt nanoparticles in chloroform obtained by reaction of ODA-capped Ag nanoparticles with hydrophobized $PtCl_6^{2-}$ ions. The inset corresponds to the SAED pattern from the hollow nanoparticles in the main image. (Reprinted with permission from ref. 60 © 2005 Royal Society of Chemistry.)

chloroform onto carbon-coated TEM grids. The particles are clearly spherical in morphology and often are multiply twinned. An analysis of a large number of Ag nanoparticles yielded an average diameter of 17.5 ± 5.4 nm. Upon addition of different amounts of hydrophobized $AuCl_4^-$ ions to the ODA-capped Ag nanoparticle solution, it is observed that the Ag surface plasmon resonance band is reduced in intensity (Fig. 13a, curves 2 and 3) and in conditions where the gold ion concentration is high (curves 4 and 5), a new absorption band appears at *ca.* 570 nm. The new absorption band arises due to reduction of $AuCl_4^-$ ions and formation of metallic gold while the concomitant loss in intensity of the Ag nanoparticle surface plasmon absorption at 410 nm is due to oxidation of silver atoms during the transmetallation reaction and deposition of the gold in the form of a shell around the silver core.[59a] The fact that the surface plasmon resonance of gold in the transmetallation reaction occurs at wavelengths slightly higher than that reported for spherical gold nanoparticles (*ca.* 520 nm) suggests the formation of shells of gold.[61] The transmetallation process described above works equally well in the reaction between ODA-capped Ag nanoparticles in chloroform and hydrophobized $PtCl_6^{2-}$ ions. Curves 1 and 2 in Fig. 13b correspond to the UV-vis absorption spectra recorded from the ODA-capped Ag nanoparticles before and after reaction with 5×10^{-5} M $PtCl_6^{2-}$ ions respectively. As in the former reaction, the silver plasmon resonance band is significantly reduced in intensity and is accompanied by a broad band in the visible region of the spectrum. Unlike in the case of gold nanoparticle formation, which exhibits a pronounced absorption in the visible region of the spectrum, Pt particles do not show such absorption. However, that the transmetallation reaction was successful is indicated by a change in color of the ODA-capped Ag nanoparticle solution from yellow (test tube

1 in inset of Fig. 13a) to brown (test tube 3, inset of Fig. 13a) after addition of hydrophobized $PtCl_6^{2-}$ ions.

Fig. 14b and c show representative TEM images recorded from ODA-capped Ag nanoparticles after reaction with 0.5×10^{-3} M hydrophobized $AuCl_4^-$ ions at different magnifications. At low magnification (Fig. 14b), it is observed that almost all the Ag nanoparticles have participated in the reaction, including particles of dimensions smaller than 20 nm. The oxidation of the silver ions and reduction of the gold ions manifests itself in the formation of a uniform Au shell and a hollow core due to leaching out of the Ag atoms as Ag^+ ions. At higher magnifications (Fig. 14c and inset), the nanoparticles are seen in much greater detail and the hollow cores in all the particles are quite prominent. The reaction of ODA-capped silver nanoparticles with hydrophobized $PtCl_6^-$ ions is equally facile and very uniform hollow Pt nanoparticles are seen at the end of this transmetallation reaction (Fig. 14d). The inset of Fig. 14d shows the SAED pattern recorded from the hollow Pt nanoparticles. The particles are clearly polycrystalline and the rings could be indexed based on the fcc structure of Pt alone. Thus, it is clear that under these reaction conditions, all the silver ions are consumed in the transmetallation reaction. The hollow Au and Pt nanoparticles are extremely stable in solution and may be readily stored as a dry powder and redispersed in a range of organic solvents.

The above studies indicate that, even in an organic environment, the transmetallation reaction occurs quite readily and, as observed in aqueous environments during previous studies,[25,59] hollow nanoparticles are formed. In earlier studies on the formation of hollow Au nanoparticles in water with sacrificial silver nanospheres, uniform shells were formed only in transmetallation reactions carried out under refluxing conditions (100 °C).[59] We observe the formation of highly uniform Au and Pt shells even under room temperature reaction conditions (Fig. 14b–d) suggested that the solvent plays an important role. This could possibly be due to ionic effects mediated by the low dielectric constant of the organic environment. While the exact process is still be elucidated, we believe the formation of hollow nanoparticles occurs by reaction of the ODA^+–$AuCl_4^-$ and $(BDSAC^+)_2$–$PtCl_6^{2-}$ ion pairs in chloroform with the surface of the ODA-capped Ag nanoparticles. The leaching out of the core in this reaction during creation of Ag^+ ions suggests that the Ag nanoparticles possess defects that facilitate reaction of the gold/platinum ions with the silver core as well as outward diffusion of the Ag^+ ions. Such pathways could be provided by twin boundaries in multiply twinned silver particles (MTP) that are observed in this study. Twin boundaries have been previously implicated in the growth of gold nanorods with gold MTPs as seeds.[62] The formation of organically redispersible hollow nanoparticles with compact and uniform shells of Au and Pt by a transmetallation reaction in one step in an organic phase has been demonstrated. Such a synthesis process is expected to be important in catalysis, biomedical and optical coating applications.

5. Conclusions

In this article, we have attempted to outline some of the new approaches developed in this laboratory on the synthesis of anisotropic flat gold nanostructures, core–shell and organically soluble hollow-shell structures. We have shown that the large-scale synthesis of highly oriented, flat gold nanosheets and nanoribbons could be synthesized by the spontaneous reduction of aqueous chloroaurate ions by HDA Langmuir monolayer. We have also shown that chloroaurate ions can be easily immobilized at the air–water interface by rendering them hydrophobic and further reduction of these chloroaurate ions, constrained to a monolayer at the air–water interface by anthranilic acid present in the subphase, results in the formation of highly anisotropic, flat gold nanostructures at the interface. These nanostructures can be transferred onto suitable solid substrates in a lamellar fashion to form thin films of desired thickness using the elegant LB technique. Variation in the crystallography of the reducing Langmuir monolayer template may lead to control over face-specific nucleation of the gold nanocrystals and is an exciting possibility. In this article we have also described the formation of core–shell nanoparticles using Keggin ions as UV-switchable and tyrosine amino acid as pH-dependable reducing agents. The use of surface-bound switchable reducing agents provided the reduction of second metal ions only on the surface of the core particles, which obviating the possibility of nucleation of fresh second metal nanoparticles in solution and using this strategy, it is possible to realize a large combination of core–shell nanostructures. We have also described the formation of organically redispersible hollow nanoparticles with compact and uniform shells of Au and Pt by a transmetallation reaction in one step in an organic phase. Such a synthesis process is expected to be important in catalysis, biomedical and optical coating applications.

Acknowledgements

A.S., S.M. and PR.S. thank the Council of Scientific and Industrial Research (CSIR) and the University Grants Commission (UGC), Govt. of India for research fellowships. This work was partially funded by grants to M.S. from the Department of Science and Technology (DST), Govt. of India and the Indo-French Centre for the Promotion of Advanced Scientific Research (IFCPAR), New Delhi and are gratefully acknowledged.

References

1 (*a*) S. Mandal, D. Roy, R. V. Chaudhari and M. Sastry, *Chem. Mater.*, 2004, **16**, 3714; (*b*) C. Qi, M. Okumura, T. Akita and M. Haruta, *Appl. Catal., A*, 2004, **263**, 19; (*c*) M. Haruta and M. Daté, *Appl. Catal., A*, 2001, **222**, 427; (*d*) M. Moreno-Manas and R. Pleixats, *Acc. Chem. Res.*, 2003, **36**, 638.

2 (*a*) T. A. Taton, C. A. Mirkin and R. L. Letsinger, *Science*, 2000, **289**, 1757; (*b*) C. J. Niemeyer, *Angew. Chem., Int. Ed.*, 2001, **40**, 4128; (*c*) Y. C. Cao, R. Jin, J. M. Nam, C. S. Thaxton and C. A. Mirkin, *J. Am. Chem. Soc.*, 2003, **125**, 14676; (*d*) R. C. Bailey, J. M. Nam, C. A. Mirkin and J. T. Hupp, *J. Am. Chem. Soc.*, 2003, **125**, 13541.

3 (*a*) N. Krasteva, I. Besnard, B. Guse, R. E. Bauer, K. Mullen, A. Yasuda and T. Vossmeyer, *Nano Lett.*, 2002, **2**, 551; (*b*) E. Katz and I. Willner, *Angew. Chem., Int. Ed.*, 2004, **43**, 6042.

4 M. L. Brongersma, J. W. Hartman and H. A. Atwater, *Phys. Rev. B*, 2000, **62**, 356.

5 (*a*) S. Sun, C. B. Murray, D. Weller, L. Folks and A. Moser, *Science*, 2000, **287**, 1989; (*b*) V. S.-Maceira, L. M. Liz-Marzan and

M. Farle, *Langmuir*, 2004, **20**, 6946; (*c*) M. Chen, J. P. Liu and S. Sun, *J. Am. Chem. Soc.*, 2004, **126**, 8394.
6 (*a*) R. Jin, Y. Cao, C. A. Mirkin, K. L. Kelly, G. C. Schatz and J. G. Zheng, *Science*, 2001, **294**, 1901; (*b*) V. Germain, J. Li, D. Ingert, Z. L. Wang and M. P. Pileni, *J. Phys. Chem. B*, 2003, **107**, 7492; (*c*) S. Chen and D. L. Carroll, *Nano Lett.*, 2002, **2**, 1003; (*d*) Y. Sun, B. Mayers and Y. Xia, *Nano Lett.*, 2003, **3**, 675; (*e*) S. Chen and D. L. Carroll, *J. Phys. Chem. B*, 2004, **108**, 5500; (*f*) I. P.-Santos and L. M. Liz-Marzan, *Nano Lett.*, 2002, **2**, 903; (*g*) N. Okada, Y. Hamanaka, A. Nakamura, I. P.-Santos and L. M. Liz-Marzan, *J. Phys. Chem. B*, 2004, **108**, 8751.
7 (*a*) T. Huang and R. W. Murray, *J. Phys. Chem. B*, 2001, **105**, 12498; (*b*) J. M. McLellan, M. Geissler and Y. Xia, *J. Am. Chem. Soc.*, 2004, **126**, 10830.
8 (*a*) T. S. Ahmadi, Z. L. Wang, T. C. Green, A. Henglein and M. A. El-Sayed, *Science*, 1996, **272**, 1924; (*b*) R. Narayanan and M. A. El-Sayed, *Nano Lett.*, 2004, **4**, 1343; (*c*) R. Narayanan and M. A. El-Sayed, *J. Am. Chem. Soc.*, 2004, **126**, 7194; (*d*) M. A. El-Sayed, *Acc. Chem. Res.*, 2001, **34**, 257.
9 (*a*) S.-W. Chung, G. Markovich and J. R. Heath, *J. Phys. Chem. B*, 1998, **102**, 6685; (*b*) Y. Sun, Y. Yin, B. T. Mayers, T. Herricks and Y. Xia, *Chem. Mater.*, 2002, **14**, 4736; (*c*) K. K. Caswell, C. M. Bender and C. J. Murphy, *Nano Lett.*, 2003, **3**, 667; (*d*) N. R. Jana, L. Gearhart and C. J. Murphy, *Chem. Commun.*, 2001, 617.
10 (*a*) K. Esumi, K. Matsuhisa and K. Torigoe, *Langmuir*, 1995, **11**, 3285; (*b*) N. R. Jana, L. Gearheart and C. J. Murphy, *J. Phys. Chem. B*, 2001, **105**, 4065; (*c*) K. R. Brown, D. G. Walter and M. J. Natan, *Chem. Mater.*, 2000, **12**, 306; (*d*) C. J. Johnson, E. Dujardin, S. A. Davis, C. J. Murphy and S. Mann, *J. Mater. Chem.*, 2002, **12**, 1765; (*e*) B. D. Busbee, S. O. Obare and C. J. Murphy, *Adv. Mater.*, 2003, **15**, 414.
11 (*a*) N. Malikova, I. Pastoriza-Santos, M. Schierhorn, N. A. Kotov and L. M. Liz-Marzan, *Langmuir*, 2002, **18**, 3694; (*b*) S. S. Shankar, A. Rai, B. Ankamwar, A. Singh and M. Sastry, *Nat. Mater.*, 2004, **3**, 482.
12 (*a*) H. Liu and A. P. Alivisatos, *Nano Lett.*, 2004, **4**, 2397; (*b*) S. Chen, Z. L. Wang, J. Ballato, S. H. Foulger and D. L. Carroll, *J. Am. Chem. Soc.*, 2003, **125**, 16186.
13 C. Loo, A. Lin, L. Hirsch, M.-H. Lee, J. Barton, N. Halas, J. West and R. Drezek, *Technol. Cancer Res. Treat.*, 2004, **3**, 33.
14 J. Chen, F. Saeki, B. J. Wiley, H. Cang, M. J. Cobb, Z.-Y. Li, L. Au, H. Zhang, M. B. Kimmey, X. Li and Y. Xia, *Nano Lett.*, 2005, DOI: 10.1021/nl047950t.
15 (*a*) S. A. Maier, M. L. Broongersma, P. G. Kik, S. Meltzer, A. A. G. Requicha, B. E. Koel and H. A. Atwater, *Adv. Mater.*, 2001, **13**, 1501; (*b*) C. Radloff and N. J. Halas, *Nano Lett.*, 2004, **4**, 1323.
16 (*a*) T. Itakura, K. Torigoe and K. Esumi, *Langmuir*, 1995, **11**, 4129; (*b*) M.-L. Wu, D.-H. Chen and T.-C. Huang, *Chem. Mater.*, 2001, **13**, 599; (*c*) M. P. Mallin and C. J. Murphy, *Nano Lett.*, 2002, **2**, 1235.
17 (*a*) M. Bruchez, Jr., M. Moronne, P. Gin, S. Weiss and A. P. Alivisatos, *Science*, 1998, **281**, 2013; (*b*) W. C. W. Chan and S. Nie, *Science*, 1998, **281**, 2016.
18 S. J. Oldenburg, R. D. Averitt, S. L. Westcott and N. J. Halas, *Chem. Phys. Lett.*, 1998, **288**, 243.
19 (*a*) Y. Jiang, S. Decker, C. Mohs and K. J. Klabunde, *J. Catal.*, 1998, **180**, 24; (*b*) J.-H. Liu, A.-Q. Wang, Y.-S. Chi, H.-P. Lin and C.-Y. Mou, *J. Phys. Chem. B.*, 2005, **109**, 40; (*c*) R. W. J. Scott, C. Sivadinarayana, O. M. Wilson, Z. Yan, D. W. Goodman and R. M. Crooks, *J. Am. Chem. Soc.*, 2005, **127**, 1380; (*d*) P. Lu, T. Teranishi, K. Asakura, M. Miyake and N. Toshima, *J. Phys. Chem. B.*, 1999, **103**, 9673.
20 J. J. Schneider, *Adv. Mater.*, 2001, **13**, 529.
21 E. P. Luther, F. F. Lange and D. S. Pearson, *J. Am. Ceram. Soc.*, 1995, **78**, 2009.
22 (*a*) G. Oldfield, T. Ung and P. Mulvaney, *Adv. Mater.*, 2000, **12**, 1519; (*b*) S. R. Hall, S. A. Davis and S. Mann, *Langmuir*, 2000, **16**, 1454; (*c*) E. Matijevic, *Langmuir*, 1994, **10**, 8.
23 F. Caruso, *Chem. Eur. J.*, 2000, **6**, 413.
24 (*a*) H. Liang, H. Zhang, J. Hu, Y. Guo, L. Wan and C. L. Bai, *Angew. Chem., Int. Ed.*, 2004, **43**, 1540; (*b*) H.-P. Liang, Y.-G. Guo, H.-M. Zhang, J.-S. Hu, L.-J. Wan and C.-L. Bai, *Chem. Commun.*, 2004, 1496.
25 (*a*) Z. Zhong, Y. Yin, B. Gates and Y. Xia, *Adv. Mater.*, 2000, **12**, 206; (*b*) Y. Yin, Y. Lu, B. Gates and Y. Xia, *Chem. Mater.*, 2001, **13**, 1146; (*c*) T. Ung, L. M. Liz-Marzan and P. Mulvaney, *Langmuir*, 1998, **14**, 3740; (*d*) F. Caruso, R. A. Caruso and H. Mohwald, *Science*, 1998, **282**, 1111.
26 Y. Sun and Y. Xia, *Nano Lett.*, 2003, **3**, 1569.
27 (*a*) M. Sastry, in *Colloids and Colloid Assemblies: Synthesis, Modification, Organization and Utilization of Colloid Particles*, ed. F. Caruso, Wiley-VCH, Berlin, Ch. 12, 2003, pp. 369–397; (*b*) F. C. Meldrum, N. A. Kotov and J. H. Fendler, *Langmuir*, 1994, **10**, 2035; (*c*) P. Ganguly, D. V. Paranjape, K. R. Patil, S. K. Chaudhari and S. T. Kshirsagar, *Indian J. Chem., Sect. A*, 1992, **31**, F42; (*d*) M. Sastry, V. Patil, K. S. Mayya, D. V. Paranjape, P. Singh and S. R. Sainkar, *Thin Solid Films*, 1998, **324**, 239; (*e*) C. Damle, A. Gole and M. Sastry, *J. Mater. Chem.*, 2000, **10**, 1389; (*f*) K. S. Mayya, V. Patil and M. Sastry, *Langmuir*, 1997, **13**, 2575; (*g*) M. Sastry, K. S. Mayya, V. Patil, D. V. Paranjape and S. G. Hegde, *J. Phys. Chem. B*, 1997, **101**, 4954; (*h*) K. S. Mayya and M. Sastry, *Langmuir*, 1998, **14**, 74; (*i*) W. Wang, X. Chen and S. Efrima, *J. Phys. Chem. B*, 1999, **103**, 7238; (*j*) J. R. Heath, C. M. Knobler and D. V. Leff, *J. Phys. Chem. B*, 1997, **101**, 189; (*k*) V. Santhanam and R. P. Andres, *Nano Lett.*, 2004, **4**, 41; (*l*) S. Chen, *Adv. Mater.*, 2000, **12**, 186.
28 J. H. Fendler and F. C. Meldrum, *Adv. Mater.*, 1995, **7**, 607.
29 (*a*) A. Swami, A. Kumar, PR. Selvakannan, S. Mandal, R. Pasricha and M. Sastry, *Chem. Mater.*, 2003, **15**, 17; (*b*) A. Swami, M. Kasture, R. Pasricha and M. Sastry, *J. Mater. Chem.*, 2004, **14**, 709.
30 (*a*) PR. Selvakannan, S. Mandal, R. Pasricha, S. D. Adyanthaya and M. Sastry, *Chem. Commun.*, 2002, 1334; (*b*) S. Mandal, PR. Selvakannan, D. Roy, R. V. Chaudhari and M. Sastry, *Chem. Commun.*, 2002, 3002.
31 G. B. Khomutov, *Colloids Surf., A*, 2002, **202**, 243.
32 M. Y. Lin, H. M. Lindsay, D. A. Weitz, R. C. Ball, R. Klein and P. Meakin, *Nature*, 1989, **339**, 360.
33 S. Mandal, S. Phadtare, PR. Selvakannan, R. Pasricha and M. Sastry, *Nanotechnology.*, 2003, **14**, 878.
34 M. P. Mallin and C. J. Murphy, *Nano Lett.*, 2002, **2**, 1235.
35 C. S. Ah, S. D. Hong and D.-J. Jang, *J. Phys. Chem. B*, 2001, **105**, 7871.
36 (*a*) J. Turkevich and G. Kim, *Science*, 1970, **169**, 873; (*b*) G. Schmid, H. West, J. Malm, J. O. Bovin and C. Grenthe, *Chem. Eur. J.*, 1996, **2**, 1099; (*c*) N. Toshima, M. Harada, Y. Yamazaki and K. Asakura, *J. Phys. Chem.*, 1992, **96**, 9927; (*d*) A. F. Lee, C. J. Baddeley, C. Hardacre, R. M. Ormerod and R. M. Lambert, *J. Phys. Chem.*, 1995, **99**, 6096; (*e*) G. Schmid, A. Lehnert, J. O. Malm and J. O. Bovin, *Angew. Chem., Int. Ed. Engl.*, 1991, **30**, 874.
37 (*a*) L. M. Liz-Marzan and A. P. Philipse, *J. Phys. Chem.*, 1995, **99**, 15120; (*b*) G. Schmid, H. West, H. Mehles and A. Lehnert, *Inorg. Chem.*, 1997, **36**, 891.
38 (*a*) M. Michaelis, A. Henglein and P. Mulvaney, *J. Phys. Chem.*, 1994, **98**, 6212; (*b*) K. Esumi, M. Wakabayashi and K. Torigoe, *Colloids Surf. A.*, 1996, **109**, 55.
39 K. Torigoe, Y. Nakajima and K. Esumi, *J. Phys. Chem.*, 1993, **97**, 8304.
40 (*a*) B. K. Teo, K. Keating and Y. H. Kao, *J. Am. Chem. Soc.*, 1987, **109**, 3494; (*b*) M. J. Hostetler, C. J. Zhong, B. K. H. Yen, J. Anderegg, S. M. Gross, S. D. Evans, M. Porter and R. W. Murray, *J. Am. Chem. Soc.*, 1998, **120**, 9396; (*c*) W. S. Han, Y. Kim and K. J. Kim, *J. Colloid Interface Sci.*, 1998, **208**, 272; (*d*) I. Lee, S. W. Han and K. Kim, *Chem. Commun.*, 2001, 1782; (*e*) Y. H. Chen and C. S. Yeh, *Chem. Commun.*, 2001, 371.
41 Y. Kobayashi, V. Salgueiriño-Maceira and L. M. Liz-Marzan, *Chem. Mater.*, 2001, **13**, 1630.
42 M. Giersig and P. Mulvaney, *Langmuir*, 1996, **12**, 4329.
43 I. Pastoriza-Santos, D. S. Koktysh, A. A. Mamedov, M. Giersig, N. A. Kotov and L. M. Liz-Marzan, *Langmuir*, 2000, **16**, 2731.
44 S. J. Oldenburg, J. B. Jackson, S. L. Westcott and N. J. Halas, *Appl. Phys. Lett.*, 1999, **75**, 2897.
45 F. Caruso, H. Lichtenfeld and H. Mohwald, *J. Am. Chem. Soc.*, 1998, **120**, 8523.
46 I. Srnova-Sloufova, F. Lednicky, A. Gemperle and J. Gemperlova, *Langmuir*, 2000, **16**, 9928.

47 (*a*) S. Mandal, PR. Selvakannan, R. Pasricha and M. Sastry, *J. Am. Chem. Soc.*, 2003, **125**, 8440; (*b*) S. Mandal, A. B. Mandale and M. Sastry, *J. Mater. Chem.*, 2004, **14**, 2868; (*c*) PR. Selvakannan, A. Swami, D. Srisathiyanarayanan, P. S. Shirude, R. Pasricha, A. B. Mandale and M. Sastry, *Langmuir*, 2004, **20**, 7825.
48 E. Papaconstantinou, *Chem. Soc. Rev.*, 1989, **18**, 1.
49 A. Troupis, A. Hiskia and E. Papaconstantinou, *Angew. Chem., Int. Ed.*, 2002, **41**, 1911.
50 S. Link, Z. I. Wang and M. A. El-Sayed, *J. Phys. Chem. B.*, 1999, **103**, 3529.
51 (*a*) M. Harada, K. Asakura and N. Toshima, *J. Phys. Chem.*, 1993, **97**, 5103; (*b*) N. Toshima and T. Yonezawa, *New J. Chem.*, 1998, 1179.
52 V. Patil, R. B. Malvankar and M. Sastry, *Langmuir*, 1999, **15**, 8197.
53 (*a*) A. Henglein, *J. Phys. Chem.*, 1993, **97**, 5457; (*b*) A. Kumar, H. Joshi, R. Pasricha, A. B. Mandale and M. Sastry, *J. Colloid Interface Sci.*, 2003, **264**, 396.
54 N. Sandhyarani and T. Pradeep, *Chem. Mater.*, 2000, **12**, 1755.
55 S. Mandal, A. Gole, N. Lala and M. Sastry, *Langmuir*, 2001, **17**, 6262.
56 S. M. Marinakos, M. F. Anderson, J. A. Ryan, L. D. Martin and D. L. Feldheim, *J. Phys. Chem. B.*, 2001, **105**, 8872.
57 L. R. Hirsch, R. J. Stafford, J. A. Bankson, S. R. Sershen, B. Rivera, R. E. Price, J. D. Hazle, N. J. Halas and J. L. West, *Proc. Natl. Acad. Sci. U. S. A.*, 2003, **100**, 13549.
58 S. U. Son, Y. Jang, J. Park, H. B. Na, H. M. Park, H. J. Yun, J. Lee and T. Hyeon, *J. Am. Chem. Soc.*, 2004, **126**, 5026.
59 (*a*) Y. Sun, B. Mayers and Y. Xia, *Adv. Mater.*, 2003, **15**, 641; (*b*) Y. Sun and Y. Xia, *J. Am. Chem. Soc.*, 2004, **126**, 3892.
60 PR. Selvakannan and M. Sastry, *Chem. Commun.*, 2005, 1684.
61 S. Lal, S. L. Westcott, R. N. Taylor, J. B. Jackson, P. Nordlander and N. J. Halas, *J. Phys. Chem. B*, 2002, **106**, 5609.
62 P. L. Gai and M. A. Harmer, *Nano Lett.*, 2002, **2**, 771.